An Ill-posed Parabolic Evolution System for Dispersive Deoxygenation-Reaeration in Waters

Mejdi Azaïez, Faker Ben Belgacem, Frédéric Hecht, Cédric Le Bot

An Ill-posed Parabolic Evolution System for Dispersive Deoxygenation-Reaeration in Waters

M. Azaïez* F. Ben Belgacem† F. Hecht‡ C. Le Bot§

May 3, 2013

Abstract

We consider an inverse problem that arises in the management of water resources and pertains to the analysis of the surface waters pollution by organic matter. Most of physical models used by engineers derive from various additions and corrections to enhance the earlier deoxygenation-reaeration model proposed by Streeter and Phelps in 1925, the unknowns being the biochemical oxygen demand (BOD) and the dissolved oxygen (DO) concentrations. The one we deal with includes Taylor's dispersion to account for the heterogeneity of the contamination in all space directions. The system we obtain is then composed of two reaction-dispersion equations. The particularity is that both Neumann and Dirichlet boundary conditions are available on the DO tracer while the BOD density is free of any condition. In fact, for real-life concerns, measurements on the dissolved oxygen are easy to obtain and to save. In the contrary, collecting data on the biochemical oxygen demand is a sensitive task and turns out to be a long-time process. The global model pursues the reconstruction of the BOD density, and especially of its flux along the boundary. Not only this problem is plainly worth studying for its own interest but it can be also a mandatory step in other applications such as the identification of the pollution sources location. The non-standard boundary conditions generate two difficulties in mathematical and computational grounds. They set up a severe coupling between both equations and they are cause of ill-posedness for the data reconstruction problem. Existence and stability fail. Identifiability is therefore the only positive result one can seek after ; it is the central purpose of the paper. We end by some computational experiences to assess the capability of the mixed finite element capability in the missing data recovery (on the biochemical oxygen demand).

Key words: deoxygenation-reaeration model, Taylor's dispersion, inverse problem, data reconstruction, identifiability.

*I2M, (UMR C.N.R.S. 5295), ENSCBP, 16 Avenue Pey-Berland, 33607 Pessac Cedex, France.
†LMAC, EA 2222, Université de Technologie de Compiègne, B.P. 20529, 60205 Compiègne Cedex, France.
‡LJLL, UMR CNRS 7598, F-75005, Paris, France.
§I2M, UMR CNRS 5295, ENSCBP, 16 Avenue Pey-Berland, 33607 Pessac Cedex, France.

1 Introduction

Oxygen is the central element in the Water Quality Assessment and is fundamental in the viability of aquatic habitat. In two or three dimensional body of waters such as lakes, bays, estuaries or even large rivers, modern models of deoxygenation and reaeration are based on parabolic boundary value problems where dispersion has been added to the earlier Streeter-Phelps model (see [24]). Streeter-Phelps' model has been firstly introduced in [20, 1925] and accounts only for reaction and advection phenomena. The study developed there has been tuned to the Ohio river, where only the longitudinal abscissa is considered. Its validity seems to be reduced to rivers and channels under the assumption that the pollution is instantaneously mixed across the whole cross-section of the river. To remediate this weakness, the 'dispersive' modeling of the contaminant transport in stream-waters has been proposed by G. I. Taylor (see [21]) to take into account the heterogeneity of the pollutant concentration in cross-sections. This correction enhances and broaden the validity of the original advective-reacting model. In the other hand, including dispersion brings about significant difficulties in mathematical analysis and scientific computations, in particular when issues related to inverse problems are intended. Readers may be referred to [17, 10, 19] for sophisticated linear and non-linear contaminant transport models.

The model we are primarily interested in relies upon the indicator $b(\cdot,\cdot)$ for the Biochemical Oxygen Demand (BOD) and on the tracer $c(\cdot,\cdot)$ for the Dissolved Oxygen (DO) concentration. The BOD density describes the rate of the oxygen to be consumed by the biodegradation of organic matter contained in the water. The DO concentration represents the amount of oxygen housed in the ambient water. Continuous organic spills (wastewater, sewage or drain discharge) in stream waters with elevated BOD depletes the DO. To translate words in mathematical equations, let us assume that the organic contaminant is discharged into a body of water occupying a domain $\Omega \subset \mathbb{R}^k, k = 2, 3$. Hence, Streeter-Phelps' equations with dispersion read as,

$$\begin{aligned} \partial_t b - \operatorname{div}(d\,\nabla b) + r\,b &= f && \text{in } (0,T)\times\Omega \\ \partial_t c - \operatorname{div}(d\,\nabla c) + r_*\,c + r\,b &= g && \text{in } (0,T)\times\Omega \\ b(t=0) &= b_0 && \text{on } \Omega \\ c(t=0) &= c_0 && \text{on } \Omega. \end{aligned} \tag{1.1}$$

The symbols $(r(\cdot), r_*(\cdot))$ stand for the reaction parameters and $d(\cdot)$ is for the dispersion coefficient. Actually, the dispersion in two or three dimensions is generally anisotropic so that it is represented by a tensor. Nevertheless, given that the analysis with isotropic dispersion does not differ at all from the anisotropic dispersion, we assume from now on that $d(\cdot)$ is a scalar function. All these physical parameters are supposed to be space-varying. The right-hand side f in (1.1), responsible for deoxygenation, describes the pollution spill, while the datum g represents the rate of oxygen supplied by the atmosphere to the river to remediate its oxygen level. The coupling term $r\,b(\cdot,\cdot)$ in the second equation is the depletion of oxygen due to an elevated $b(\cdot,\cdot)$. This says that the river will suffer from high deoxygenation due to high level of BOD which poses serious threats to marine environment. The initial state (b_0, c_0) is often defined by $(0, c_S)$. At the time origin, the river is not polluted and the dissolved oxygen is at the saturation level c_S. To be complete

with the model, boundary conditions are required. Neumann conditions are natural, the fluxes $(d\partial_n b, d\partial_n c)$ are therefore prescribed along the boundary. The related problem has then a triangular structure and may be uncoupled. Indeed, the scalar equation involving the density $b(\cdot,\cdot)$ may be solved independently ; it is well-posed. Afterwards, we turn to the equation on $c(\cdot,\cdot)$, for which the oxygen depletion term acts as a sink source. It is also well-posed and can be solved easily.

The problem we focus on here is pretty different and arises when abundant data are collected on the DO concentration $c(\cdot,\cdot)$. The counterpart is that no measurements are available on the BOD density $b(\cdot,\cdot)$. The boundary conditions to deal with henceforth may be expressed by

$$\begin{aligned} c &= \zeta \qquad \text{on } (0,T)\times\partial\Omega \\ d\partial_n c &= \xi \qquad \text{on } (0,T)\times\partial\Omega. \end{aligned} \tag{1.2}$$

The data (ζ,ξ) are given. Notice that this is not a rare occurrence. In fact, if polluting agents affect estuaries through their bank then measurements on the DO concentration $c(\cdot,\cdot)$ can instantaneously be performed along the border. Similar data on the BOD density $b(\cdot,\cdot)$ are harder to collect and tedious to obtain. Protecting the environment from the effects of dangerous contaminant unloads urges people committed to to satisfy themselves with the available information, make appropriate decisions and implement them as quickly as possible. Numerical software are affordable tools for the reconstruction of the missing data on b and $(D\partial_n b)$ along the border. This may help hydrological engineers enhancing and increase the amount of information they dispose of to proceed efficiently with the accidental spills.
A major effect caused by the non-standard boundary conditions (1.2) is that the triangular structure of the problem is definitely lost. The depletion term $rb(\cdot,\cdot)$ generates a strong coupling between both equations. The second important issue consists in the deep change in the nature of the problem (1.1)-(1.2) because its well-posed is thus broken. The ill-posedness of the problem has been illustrated in [3] (see also [4]). Existence and stability fail. Only the identifiability has been successfully stated there in the particular case of constant reaction parameters. In a more recent work on the steady problem, expected to be well-posed, have emerged some surprising remarks. Complications of the mathematical analysis are tremendously increased when the reaction parameters become space-dependent (see [5]). By the way, all our attempts to state existence results for arbitrary kinetic parameters fell short and to our knowledge the issue is still open in the steady case. The positive results in [5] prevail only when the gap between the extrema of the square root of the ratio function $\sqrt{r_*/r}$ does not exceed two. For a while, we suspected this limitation to apply as well to the identifiability for the unsteady data completion problem (1.1)-(1.2). Nothing could be less true, by chance. This will be corroborated by the analysis we propose here.

The purpose is hence is to obtain the only possible positive result, the identifiability for the unsteady dispersive Streeter-Phelps model (1.1)-(1.2). The chief tool we use is a uniqueness result by A. Pazy proven in [18, Chapter 4, Theorem 1.2] in an abstract framework of semi-group theory. The preamble to the application of such a powerful result consists in suitable a-priori estimates on the resolvent of the spacial operator underlying the time-dependent problem. We shall then carry out a full study of the quasi-steady version of (1.1)-(1.2) where the time derivatives $(\partial_t b, \partial_t c)$ are

replaced by $(\lambda b, \lambda c)$ for a positive real number λ. This is the subject of Section 2. It turns out to be the most difficult part. We resume the variational methodology introduced in [4]. A saddle-point problem emerges then. The major point with this (saddle-point) problem is the lack of symmetry. A specific abstract framework has been developed in [16, 6] for the non-symmetric saddle-point problems. The keys to their analysis are several inf-sup conditions some of which are far from being obvious to establish. This task is brought to a successful conclusion here, *for large values of* λ. This result allows us to state the required estimates on the resolvent of the quasi-steady problem. Based on these estimates, Section 3 explains how Pazy's theorem provides the identifiability. Section 4 is dedicated to a brief description of the mixed finite element method applied to the approximation of the quasi-steady problem. To close, we perform and comment in Section 5 some numerical experiences to solve the steady and unsteady versions of problem (1.1)-(1.2).

FUNCTIONAL NOTATION. The Lebesgue space of square integrable functions over Ω is denoted by $L^2(\Omega)$, and $(\cdot,\cdot)$ stands for the scalar product. The Sobolev space $H^1(\Omega)$ contains all the functions that belong to $L^2(\Omega)$ so as their first-order derivatives. We also denote by $H^1_0(\Omega)$, the subspace of $H^1(\Omega)$ made of all functions whose traces on $\partial\Omega$ vanish. The dual space of $H^1_0(\Omega)$ is $H^{-1}(\Omega)$ and the duality pairing is represented by $\langle\cdot,\cdot\rangle_{H^{-1},H^1_0}$. We refer to [1] for more details on these functional spaces. Although not necessary, we shall use for convenience the weighted norms

$$\|\chi\|_{L^2_r(\Omega)} = (\chi, \chi\, r)^{1/2} \qquad \text{and} \qquad \|\varphi\|_{L^2_{r_*}(\Omega)} = (\varphi, \varphi\, r_*)^{1/2}.$$

2 The quasi-steady model

We follow the methodology of [4] for the identification result for (1.1)-(1.2), the aim being to apply Pazy's uniqueness theorem for the time-dependent equation. It is therefore mandatory to study the related quasi-steady boundary value problem ; the time derivatives $(\partial_t b, \partial_t c)$ are hence replaced by $(\lambda b, \lambda c)$ for a positive real number λ. The generalization we pursue, compared to [4], is concerned with the kinetic terms in the dispersive Streeter and Phelps model where the reaction coefficients $r(\cdot)$, $r_*(\cdot)$ are dependent on the space variable. Unexpectedly, this is source of substantial difficulties. We refer to [5] where this intricating issue is firstly reported. To proceed, let us first write down the quasi-steady problem

$$\begin{aligned} \lambda b - \operatorname{div}(d\,\nabla b) + r\, b &= f \qquad \text{in } \Omega \\ \lambda c - \operatorname{div}(d\,\nabla c) + r_*\, c + r\, b &= g \qquad \text{in } \Omega \\ c &= 0 \qquad \text{on } \partial\Omega \\ d\,\partial_n c &= 0 \qquad \text{on } \partial\Omega. \end{aligned} \tag{2.1}$$

This has been studied in [4], when (r, r_*) are constants. A suitable functional framework has been led down there. Existence and uniqueness results have been stated. When the reaction coefficients are space-dependent things turn out to be surprisingly very different and much more complicated. As a matter of fact, in the steady case that is when $\lambda = 0$, we are able to show the well-posedness only for a reduced class of the parameters $r(\cdot)$ and $r_*(\cdot)$ (see [5]). The nice feature here is that this limitation is found to be not effective for the quasi-steady case for large values of λ. A direct consequence is that the identifiability result we have primarily in mind holds for the unsteady problem

(1.1)-(1.2) without any restriction on the reaction parameters.

Prior to the technical developments, we need supplementary regularity assumptions on the physical parameters. Reaction coefficients $r(\cdot)$ and $r_*(\cdot)$ are piecewise continuous on $\overline{\Omega}$ and also that there exist positive real-numbers $r_\sharp$, $d_\flat$ and $d_\sharp$ such that

$$\forall \boldsymbol{x} \in \overline{\Omega}, \qquad 0 < r(\boldsymbol{x}), r_*(\boldsymbol{x}) \leq r_\sharp \quad \text{and} \quad d_\flat \leq d(\boldsymbol{x}) \leq d_\sharp.$$

2.1 The variational framework

A suitable functional framework should be available to put problem (2.1) under a variational form. We adopt here the one used in [4] and introduced earlier in [7] for the vorticity-streamfunction formulation of the Stokes problem. Let us hence consider the non-standard Hilbert space

$$\mathbb{V} = \Big\{ \chi \in L^2(\Omega); \quad \operatorname{div}(d\,\nabla\chi) \in H^{-1}(\Omega) \Big\},$$

endowed with the graph norm

$$\|\chi\|_{\mathbb{V}} = \Big(\|\operatorname{div}(d\,\nabla\chi)\|^2_{H^{-1}(\Omega)} + \|\chi\|^2_{L^2_r(\Omega)} \Big)^{1/2}.$$

To step ahead, some additional notations and definitions may help us to present the technical results we have in mind. We define hence three bilinear forms, for all $\chi \in \mathbb{V}, \varphi \in \mathbb{V}, \psi \in H^1_0(\Omega)$

$$\begin{aligned} a(\chi,\varphi) &= (r\,\chi,\varphi), \\ m(\psi,\varphi) &= \langle -\operatorname{div}(d\,\nabla\varphi) + (\lambda + r)\,\varphi, \psi \,\rangle_{H^{-1},H^1_0}, \\ m_*(\psi,\varphi) &= \langle -\operatorname{div}(d\,\nabla\varphi) + (\lambda + r_*)\,\varphi, \psi \,\rangle_{H^{-1},H^1_0}. \end{aligned}$$

They are all continuous, $a(\cdot,\cdot)$ on $\mathbb{V}\times\mathbb{V}$ and $m(\cdot,\cdot)$ and $m_*(\cdot,\cdot)$ on $H^1_0(\Omega)\times\mathbb{V}$.

Now, the mixed variational problem may be expressed in terms of these bilinear forms as: *Find* (b,c) *in* $\mathbb{V}\times H^1_0(\Omega)$ *such that*

$$\begin{aligned} \forall \psi \in H^1_0(\Omega), \qquad & m\,(\psi,b) = \langle f,\psi\rangle_{H^{-1},H^1_0}, \\ \forall \varphi \in \mathbb{V}, \qquad & m_*(c,\varphi) + a(b,\varphi) = (g,\varphi). \end{aligned} \tag{2.2}$$

This is a linear saddle-point problem. It is non-symmetric because $m(\cdot,\cdot)$ and $m_*(\cdot,\cdot)$ do not coincide. Indeed, $r(\cdot)$ and $r_*(\cdot)$ are typically different. Several worthy manuscripts and papers has been dedicated to the abstract linear saddle-point problems. We refer to [9] for a general treatise and to [16] (see also [6]) which deals specifically with the non-symmetric problems.

2.2 Uniqueness

In the steady case that is $\lambda = 0$ only a partial result has been obtained in [5]. The well posedness is proved there for a limited class of the kinetic parameters $(r(\cdot), r_*(\cdot))$. The salient fact is that, when we come to the quasi-steady problem (2.2), stating existence and uniqueness results turns out to be possible for arbitrary coefficients $(r(\cdot), r_*(\cdot))$, provided that λ is sufficiently large. To understand how things operate, when λ is large, we propose to look at the proof of the uniqueness.

Lemma 2.1 *Problem* (2.2) *has at most one solution for large values of* λ.

Proof: Consider that the data are homogeneous, then $(f, g) = (0, 0)$. We hope to check that $(b, c) = (0, 0)$ is the unique solution. We proceed by choosing $\psi = c$ and $\varphi = b$ in (2.2). Subtracting both equations yields

$$((r_* - r)b, c) + \|b\|^2_{L^2_r(\Omega)} = 0.$$

This formula allows to derive the following bound

$$\|b\|_{L^2_r(\Omega)} \leq \beta \|c\|_{L^2_{r_*}(\Omega)}, \tag{2.3}$$

for some real-number $\beta > 0$, that does not depends on λ. Then, back to the second equation with $\varphi = c$, we obtain that

$$\|d^{1/2}\ \nabla c\|^2_{L^2(\Omega)^2} + \lambda \|c\|^2_{L^2(\Omega)} + \|c\|^2_{L^2_{r_*}(\Omega)} = -(rb, c).$$

Using the bound (2.3) allows for

$$\|d^{1/2}\ \nabla c\|^2_{L^2(\Omega)^2} + \lambda \|c\|^2_{L^2(\Omega)} + \|c\|^2_{L^2_{r_*}(\Omega)} \leq \beta_* \|c\|^2_{L^2_{r_*}(\Omega)}.$$

Once again, the constant β_* is independent of λ. Now, if λ is large enough then $c(\cdot) = 0$ and we have straightforwardly $b(\cdot) = 0$. The proof is complete.

∎

2.3 Existence

After the uniqueness, we investigate the existence. The basic tool is the fulfillment of inf-sup conditions on the bilinear forms involved in the variational formulation (see [16], [7]). We start by checking the mixed forms $m(\cdot, \cdot)$ and $m_*(\cdot, \cdot)$. The proofs of the following lemma are detailed in [4].

Lemma 2.2 ([4, Lemma 3.2]) *The following inf-sup conditions hold*

$$\forall \psi \in H^1_0(\Omega), \quad \sup_{\varphi \in \mathbb{V}} \frac{m(\psi, \varphi)}{\|\varphi\|_{\mathbb{V}}} \geq \alpha \|\psi\|_{H^1(\Omega)}.$$

$$\forall \psi \in H^1_0(\Omega), \quad \sup_{\varphi \in \mathbb{V}} \frac{m_*(\psi, \varphi)}{\|\varphi\|_{\mathbb{V}}} \geq \alpha \|\psi\|_{H^1(\Omega)}.$$

The constant α *may be chosen independent of* λ.

Things a less simple for the bilinear form $a(\cdot, \cdot)$ which must satisfy an inf-sup condition and a positivity property on both null-spaces of the forms $m(\cdot, \cdot)$ and $m_*(\cdot, \cdot)$. They are defined to be

$$\mathcal{N} = \Big\{ \varphi \in \mathbb{V}; \quad \forall \psi \in H^1_0(\Omega),\ m(\psi, \varphi) = 0 \Big\}$$

$$\mathcal{N}_* = \Big\{ \chi \in \mathbb{V}; \quad \forall \psi \in H^1_0(\Omega),\ m_*(\psi, \chi) = 0 \Big\}.$$

The following statements

$$\mathcal{N} = \Big\{ \varphi \in \mathbb{V}, \quad -\operatorname{div}(d \nabla \varphi) + (\lambda + r)\, \varphi = 0 \text{ in } \Omega \Big\},$$

$$\mathcal{N}_* = \Big\{ \chi \in \mathbb{V}, \quad -\operatorname{div}(d \nabla \chi) + (\lambda + r_*)\, \chi = 0 \text{ in } \Omega \Big\}.$$

are straightforward. Both spaces are closed subspaces in $\mathbb{V}$ and have thus Hilbertian structures, when endowed with $\| \cdot \|_{\mathbb{V}}$.

Remark 2.3 The norm $\|\cdot\|_{L^2_r(\Omega)}$ (resp. $\|\cdot\|_{L^2_{r_*}(\Omega)}$) is equivalent to $\|\cdot\|_{\mathbb{V}}$ in both spaces $\mathcal{N}$ and $\mathcal{N}_*$. The equivalence constants are obviously functions of λ.

Notice if $f = 0$ then problem (2.2) is equivalent to the reduced one: *Find b in $\mathcal{N}$ such that*

$$\forall \varphi \in \mathcal{N}_*, \qquad a(b, \varphi) = (g, \varphi). \tag{2.4}$$

The analysis of this equation may be brought to a conclusion if the couple of inf-sup conditions we look for succeed. Accordingly, the main purpose is thus to bound from below the following inf-sup quantities

$$\inf_{\varphi\in\mathcal{N}} \sup_{\chi\in\mathcal{N}_*} \frac{a(\varphi,\chi)}{\|\varphi\|_{\mathbb{V}}\|\chi\|_{\mathbb{V}}} \qquad \text{and} \qquad \inf_{\chi\in\mathcal{N}_*} \sup_{\varphi\in\mathcal{N}} \frac{a(\varphi,\chi)}{\|\varphi\|_{\mathbb{V}}\|\chi\|_{\mathbb{V}}}.$$

An intermediary result may help one doing so. We construct an isomorphism $\mathcal{K}$ between $\mathcal{N}$ and $\mathcal{N}_*$ as follows. Let us φ be in $\mathcal{N}$, define θ in $H^1_0(\Omega)$ as the unique solution of

$$-\operatorname{div}(d\,\nabla\theta) + (\lambda + r_*)\theta = (r - r_*)\,\varphi \qquad \text{in } \Omega. \tag{2.5}$$

Then, set $\mathcal{K}\varphi = \theta + \varphi$. Clearly, the function $\mathcal{K}\varphi$ belongs to $\mathcal{N}_*$.

Lemma 2.4 *The following inequalities hold*

$$\forall \varphi \in \mathcal{N}, \qquad \sigma_\flat \|\varphi\|_{L^2_r(\Omega)} \le \|\mathcal{K}\varphi\|_{L^2_{r_*}(\Omega)} \le \sigma_\sharp \|\varphi\|_{L^2_r(\Omega)},$$

The constants $\sigma_\flat$ and $\sigma_\sharp$ depend only on the reactions $(r(\cdot), r_*(\cdot))$.

Proof: The proof follows the same lines as [4, Lemma 3.3]. The slight difference is to account for the term dependent of λ which does not arise any significant obstacle. The details are skipped over. We emphasize only on the important fact that the constants $\sigma_\flat$ and $\sigma_\sharp$ may be chosen independent of λ. ∎

This lemma is of a great help in the preparation of the harder part: establishing the inf-sup conditions on $a(\cdot,\cdot)$. We have a preliminary result

Lemma 2.5 *Let $\lambda_\flat$ be a real-number sufficiently large. Then,the following inf-sup conditions holds, for any $\lambda \ge \lambda_\flat$,*

$$\forall \varphi \in \mathcal{N}, \quad \sup_{\chi\in\mathcal{N}_*} \frac{a(\varphi,\chi)}{\|\chi\|_{L^2_{r_*}(\Omega)}} \ge \eta\, \|\varphi\|_{L^2_r(\Omega)},$$
$$\forall \chi \in \mathcal{N}_*, \quad \sup_{\varphi\in\mathcal{N}} \frac{a(\varphi,\chi)}{\|\varphi\|_{L^2_r(\Omega)}} \ge \eta\, \|\chi\|_{L^2_{r_*}(\Omega)}.$$

The constant η depends on $\lambda_\flat$. It is uniform for $\lambda \ge \lambda_\flat$.

Proof: Let φ be given in $\mathcal{N}$, we set $\chi = \mathcal{K}\varphi$. Then χ lies in $\mathcal{N}_*$. The difference function $\theta = (\varphi - \chi)$ belongs to $H^1_0(\Omega)$ and satisfies

$$-\operatorname{div}(d\,\nabla\theta) + (\lambda + r)\,\varphi - (\lambda + r_*)\,\chi = 0 \qquad \text{in } \Omega.$$

This equation stems from (2.5). Multiplying by θ and applying Green's formula we obtain

$$\begin{aligned}\|d^{1/2}\nabla\theta\|^2_{L^2(\Omega)^k} + \|\varphi\|^2_{L^2_{r+\lambda}(\Omega)} + \|\chi\|^2_{L^2_{r_*+\lambda}(\Omega)} &= ((r+\lambda)\,\chi,\varphi) + ((r_*+\lambda)\,\chi,\varphi)\\ &= a(\chi,\varphi) + ((r_*+2\lambda)\,\chi,\varphi),\end{aligned}$$

Using Young's inequality $ts \le t^2 + s^2/4$, results in the following

$$a(\chi,\varphi) + (\frac{(r_*+2\lambda)^2}{4(r_*+\lambda)}\,\varphi,\varphi) + \|\chi\|^2_{L^2_{r_*+\lambda}(\Omega)} \ge \|\varphi\|^2_{L^2_{r+\lambda}(\Omega)} + \|\chi\|^2_{L^2_{r_*+\lambda}(\Omega)}$$

whence

$$a(\chi,\varphi) \ge \int_\Omega \left[1 - \frac{(r_*+2\lambda)^2}{4(r+\lambda)(r_*+\lambda)}\right](r+\lambda)\varphi^2\,d\boldsymbol{x} = \int_\Omega \left[\frac{r_*(4r-r_*)+4r\lambda}{4(r_*+\lambda)}\right]\varphi^2\,d\boldsymbol{x}.$$

Assume that $\lambda_\flat$ is large enough, then there exists a constant $\beta = \beta(\lambda_\flat) \in]0,1[$ such that for all $\lambda \ge \lambda_\flat$ there hold that

$$a(\chi,\varphi) \ge \beta \int_\Omega r\varphi^2\,d\boldsymbol{x} \ge \beta\|\varphi\|^2_{L^2_r(\Omega)}.$$

Now, owing to the estimate by Lemma 2.5, we deduce that

$$\frac{a(\chi,\varphi)}{\|\chi\|_{L^2_{r_*}(\Omega)}} \ge \frac{\beta}{\sigma_\sharp}\|\varphi\|_{L^2_r(\Omega)}.$$

This provides the first inf-sup condition. The second one is checked out following the same arguments. ∎

Remark 2.6 According to the proof of Lemma 2.5, the steady case ($\lambda = 0$) suffers from limitations. The proof still works for the class of kinetic coefficients (r, r_*) subjected to the restriction that the ratio function $\sqrt{r_*/r}$ is lower then 4. In reality, that result has been extended for a broader class of (r, r_*) (see [5]).

Lemma 2.7 *Let $\lambda_\flat$ be a real-number sufficiently large. Then,the following inf-sup conditions holds, for any $\lambda \ge \lambda_\flat$,*

$$\begin{aligned}\forall\varphi \in \mathcal{N}, \quad \sup_{\chi\in\mathcal{N}_*} \frac{a(\varphi,\chi)}{\|\chi\|_{\mathbb{V}}} &\ge \eta'_\lambda\,\|\varphi\|_{\mathbb{V}},\\ \forall\chi \in \mathcal{N}_*, \quad \sup_{\varphi\in\mathcal{N}} \frac{a(\varphi,\chi)}{\|\varphi\|_{\mathbb{V}}} &\ge \eta'_\lambda\,\|\chi\|_{\mathbb{V}}.\end{aligned}$$

The constant η'_λ is dependent on λ.

Proof: It is directly issued from Lemma 2.5 and Remark 2.3. ∎

Remark 2.8 It can be shown that the constant η_λ decays like $\frac{1}{\lambda^2}$, for growing λ.

Sufficient tools to state and prove the the existence for the mixed quasi-steady problem (2.2) are now available. The following is a direct consequence of Lemmas 2.2 and 2.7.

Proposition 2.9 *Problem* (2.2) *has a unique solution* (b, c) *in* $\mathbb{V} \times H_0^1(\Omega)$*, for large values of* λ*. Moreover this solution satisfies*

$$\|b\|_{\mathbb{V}} + \|c\|_{H^1(\Omega)} \leq C_\lambda(\|f\|_{H^{-1}(\Omega)} + \|g\|_{L^2(\Omega)}).$$

The constant C_λ *depends on* λ*.*

2.4 Stability

Deriving a-priori estimates on the solution of (2.2) is possible from the previous section. But, the very point we are devoted to look at is the behavior of the stability constant with respect to λ. That is the reason why we choose to handle the issue in a separate paragraph.

Proposition 2.10 *Assume that* λ *is large enough. Then, we have that*

$$\|b\|_{L^2(\Omega)} + \lambda\|c\|_{L^2(\Omega)} \leq C(\|f\|_{H^{-1}(\Omega)} + \|g\|_{L^2(\Omega)}).$$

The constant C *does not depend on* λ*.*

Proof: We start by the case $(f = 0)$. Applying the first inf-sup condition in Lemma 2.5 to the reduced problem (2.4), we derive that

$$\|b\|_{L^2_r(\Omega)} \leq C\|g\|_{L^2(\Omega)}.$$

The second equation of problem (2.2), with $\varphi = c$, provides that

$$\|d^{1/2}\ \nabla c\|^2_{L^2(\Omega)^2} + \lambda\|c\|^2_{L^2(\Omega)} + \|c\|^2_{L^2_{r_*}(\Omega)} = -(rb, c) + (g, c).$$

This, together with the bound in b, yields in particular that

$$\lambda\|c\|_{L^2(\Omega)} \leq C\|g\|_{L^2(\Omega)}.$$

Extension to the case $(f \neq 0)$ is based on the superposition principle and is easy to realize. The proof is complete. ∎

Remark 2.11 It may also be checked out that

$$\|b\|_{\mathbb{V}} + \lambda\|c\|_{H^1(\Omega)} \leq C\lambda(\|f\|_{H^{-1}(\Omega)} + \|g\|_{L^2(\Omega)}).$$

3 Identifiability for the unsteady problem

The central statement we are about to prove is the identifiability for the time-dependent dispersive Streeter-Phelps model (1.1)-(1.2). The tool to establish uniqueness is a suitable theorem worked out by A. Pazy in his treatise on semi-groups of linear operators (see [18]).

The methodology we follows starts by setting the Hilbert space $\mathbb{H}(\Omega) = L^2(\Omega) \times L^2(\Omega)$. Then, assume given (f, g) in $L^2(0, T, W(\Omega))$, we consider the abstract time-dependent parabolic system

$$\partial_t \begin{pmatrix} b \\ c \end{pmatrix} + A \begin{pmatrix} b \\ c \end{pmatrix} = \begin{pmatrix} f \\ g \end{pmatrix}. \tag{3.1}$$

The operator A is an linear and unbounded with the domain

$$D(A) = \Big\{(\varphi,\psi) \in \mathbb{V} \times H_0^1(\Omega), \quad \operatorname{div}(d\,\nabla\varphi) \in L^2(\Omega), \\ \operatorname{div}(d\,\nabla\psi) \in L^2(\Omega), \quad (d\partial_n\psi)_{|\partial\Omega} = 0\Big\} \subset \mathbb{H}(\Omega).$$

It is defined by

$$A\begin{pmatrix}\varphi\\ \psi\end{pmatrix} = \begin{pmatrix} -\operatorname{div}(d\,\nabla\varphi) + r\varphi \\ -\operatorname{div}(d\,\nabla\psi) + r_*\psi + r\varphi\end{pmatrix}.$$

The domain $D(A)$ is dense in $\mathbb{H}(\Omega)$ and it is readily checked that the graph of A is closed. A is thus a closed operator with a dense domain. Next, the properties of the differential equation (3.1) relies basically on the resolvent $\mathcal{R}(\lambda) = (\lambda + A)^{-1}$. So let us first state that, for large λ, the operator $\mathcal{R}(\lambda)$ is well defined in $\mathbb{H}(\Omega)$.

Lemma 3.1 *Let (f, g) be given in $\mathbb{H}(\Omega)$. Problem (2.1) has a unique solution (b, c) that belongs to $D(A)$, for large values of λ.*

Proof: Let (f, g) be given in $\mathbb{H}(\Omega)$. First, we call for Proposition 2.9. The variational problem (2.2) admits then a unique solution (b, c) in $\mathbb{V} \times H_0^1(\Omega)$. Back to the strong formulation (2.1), we see that $(\operatorname{div}(d\,\nabla c))$ belongs actually to $L^2(\Omega)$. Besides, the homogeneous Neumann condition $(d\partial_n\psi) = 0$ holds on the boundary $\partial\Omega$. Finally, it remains to see whether $(\operatorname{div}(d\,\nabla b))$ lies in $L^2(\Omega)$. This ensues straightforwardly from the fact that f is taken in $L^2(\Omega)$ here. The proof is complete. ∎

The crucial point is the stability of the resolvent in the framework of $\mathbb{H}(\Omega)$. The following statement holds

Proposition 3.2 *Assume that λ is large enough. Then we have that*

$$\|\mathcal{R}(\lambda)(f, g)\|_{\mathbb{H}(\Omega)} \leq C\|(f, g)\|_{\mathbb{H}(\Omega)}.$$

The constant C does not depend on λ.

Proof: This is directly issued from Proposition 3.2 ∎

Remark 3.3 Observe that the estimate on the resolvent $\mathcal{R}(\lambda)$ is incompatible with Hille-Yosida's theory. This was of course expected since, as previously observed in [4], our problem is ill-posed.

Equipped with the suitable mathematical tools, we are able to complete the proof of the uniqueness for the time-dependent pollution problem (1.1). We emphasize the fact that no particular assumptions are required on the kinetic parameters $(r(\cdot), r_*(\cdot))$ to obtain such a result.

Theorem 3.4 *Problem (1.1) has at most one solution in $\mathscr{C}([0, T]; W(\Omega))$.*

Proof: Owing to the bound on the resolvent $\mathcal{R}(\lambda)$ stated in Proposition 3.2, we have that

$$\lim_{\lambda\to\infty} \frac{1}{\lambda} \log \|\mathcal{R}(\lambda)\|_{(W(\Omega)\to W(\Omega))} = 0.$$

Then, Pazy's Theorem (see [18, Chapter 4, Theorem 1.2]) applies and provides the uniqueness. This completes the proof. ∎

4 A mixed finite element method

Prior to any numerical discussion, we briefly describe the finite element discretization we use in our computations for quasi-steady problem (2.1) and then for the unsteady model (1.1). The quasi-steady version (2.1) looks like the vorticity/stream-function problem. As soundly remarked in [2], users of linear finite elements are expected to face some inaccuracy in particular on the variable $b(\cdot)$. A relevant remedy to this sort of numerical locking is to introduce some regularization procedures to improve the reliability of the finite element discretization. The one we use is fully assessed in [2].

Now, assume the domain Ω to be polygonal. It is divided into a finite number of triangles. Then, we introduce a regular family $(\mathcal{T}_h)_h$ of triangulations of Ω.

- Ω is the union of all elements of $\mathcal{T}_h$;
- The intersection of two different elements of $\mathcal{T}_h$, if not empty, is a vertex or a whole edge of both of them;
- The ratio of the diameter h_K of any element K of $\mathcal{T}_h$ to the diameter of its inscribed circle is smaller than a constant σ independent of h.

The mesh-size h is the maximum of the diameters h_K. We refer to [11, 8] for the basics of the finite element method.
Next, we consider the discrete spaces $\mathbb{V}_h \subset \mathbb{V}$ and $\mathbb{H}_h \subset H_0^1(\Omega)$, defined by

$$\mathbb{V}_h = \Big\{ \chi_h \in H^1(\Omega); \quad \forall K \in \mathcal{T}_h, \ \ (\chi_h)_{|K} \in \mathcal{P}_1(K) \Big\}, \qquad \mathbb{H}_h = \mathbb{V}_h \cap H_0^1(\Omega),$$

where $\mathcal{P}_1(K)$ stands for the space of restrictions to K of affine functions on $\mathbb{R}^2$. The first discrete problem in the quasi-steady case is constructed from (2.2) by the Ritz–Galerkin method. It reads as: *find* (b_h, c_h) *in* $\mathbb{V}_h \times \mathbb{H}_h$ *fulfilling*

$$\begin{aligned} &\forall \psi_h \in \mathbb{H}_h, \qquad m_h\,(\psi_h, b_h) = \langle f, \psi_h \rangle_{H^{-1}, H_0^1}, \\ &\forall \varphi_h \in \mathbb{V}_h, \qquad m_{*,h}(c_h, \varphi_h) + a_{\rho,h}(b_h, \varphi_h) = (g, \varphi_h), \end{aligned} \tag{4.1}$$

where now, the mixed bilinear forms $m_h(\cdot,\cdot)$ and $m_{*,h}(\cdot,\cdot)$ have different forms, compared to the exact ones,

$$\begin{aligned} &\forall (\psi_h, \varphi_h) \in \mathbb{H}_h \times \mathbb{V}_h, \qquad m_h(\psi_h, \varphi_h) = (d\,\nabla\varphi_h, \nabla\psi_h) + ((\lambda + r)\,\varphi_h, \psi_h), \\ &\forall (\psi_h, \varphi_h) \in \mathbb{H}_h \times \mathbb{V}_h, \qquad m_{*,h}(\psi_h, \varphi_h) = (d\,\nabla\varphi_h, \nabla\psi_h) + ((\lambda + r_*)\,\varphi_h, \psi_h). \end{aligned}$$

The augmented bilinear form $a_{\rho,h}(\cdot,\cdot)$ is expressed as

$$\begin{aligned} a_{\rho,h}(\chi_h, \varphi_h) = a(\chi_h, \varphi_h) &+ \rho \sum_{e \in \mathcal{E}_h} h_e \int_e [d\partial_n \chi_h]_e(\tau) [d\partial_n \varphi_h]_e(\tau)\, d\tau \\ &+ \rho \sum_{K \in \mathcal{T}_h} \mathrm{meas}(K) \int_K \mathrm{div}\,(d\,\nabla\chi_h)\,\mathrm{div}\,(d\,\nabla\varphi_h)\, d\boldsymbol{x}. \end{aligned}$$

$\mathcal{E}_h$ stands for the set of all edges of elements of $\mathcal{T}_h$ which are not located in $\partial\Omega$. The parameter ρ is a positive real number called the regularization coefficient. Note that the current form of the bilinear

forms $m_h(\cdot,\cdot)$ and $m_{*,h}(\cdot,\cdot)$ coincide with $m(\cdot,\cdot)$ and $m_*(\cdot,\cdot)$, respectively, on $H_0^1(\Omega)\times H^1(\Omega)$, and by then on $\mathbb{H}_h\times\mathbb{V}_h$. In [5] is carried out the numerical analysis of the regularized mixed finite element method in the linear case. The convergence estimates established there are the following

$$\|b-b_h\|_{L^2(\Omega)}+\sqrt{\rho}\,\|b-b_h\|_{\mathbb{V}}+\|c-c_h\|_{H^1(\Omega)}\leq Ch(|b|_{H^2\Omega)}+|c|_{H^2(\Omega)}).$$

Thus, they predict that the errors $\|b-b_h\|_{\mathbb{V}}$ would be strongly affected by the choice of ρ while $\|c-c_h\|_{H^1(\Omega)}$ seem to be less sensitive to ρ. For a suitable chosen ρ, both errors decreases like h when the mesh size gets small.

Remark 4.1 The regularization procedure seems mandatory for the linear finite elements otherwise the computations may lead to some erratic solutions, in particular the density $b_h(\cdot)$ may suffer from undesired oscillation along the boundary. Higher order finite elements are expected to preserve their good behaviors and users can spared form using any regularization without endangering the accuracy.

Remark 4.2 In order to put the mixed problem under a matrix form, we denote by $\boldsymbol{b}$ and $\boldsymbol{c}$ the vectors of unknowns for the BOD concentration b_h and the DO density c_h. The degrees of freedom in $\boldsymbol{b}$ are the values of b_h at all finite elements vertices and those of $\boldsymbol{c}$ made of the values of c_h at the internal vertices , not located on $\partial\Omega$. The problem (4.1) results into a linear system:

$$\begin{pmatrix} A_\rho & M_* \\ M & 0 \end{pmatrix}\begin{pmatrix} \boldsymbol{b} \\ \boldsymbol{c} \end{pmatrix}=\begin{pmatrix} \boldsymbol{g} \\ \boldsymbol{f} \end{pmatrix}, \tag{4.2}$$

The matrix A_ρ is symmetric positive definite while the matrices M and M_* are related to the mixed bilinear forms $m_h(\cdot,\cdot)$ and $m_{*,h}(\cdot,\cdot)$ and are rectangular. Owing to the analysis realized here, the global matrix is square and invertible. Thus, it can be solved either directly. We use `UMFPack` or `sparsesolver` incorporated in `Freefem++`.

When it comes to the approximation of the time-dependent problem (1.1), a time marching scheme has to be combined with the stabilized finite element method. Let then τ be time step and $T=n^*\tau$. We denote (b_h^n,c_h^n) the approximation of $(b(n\tau,\cdot),c(n\tau,\cdot))$. We opt for the implicit Euler time scheme. The problem to solve is thus expressed as follows: *find the sequence* $((b_h^n)_n,(c_h^n)_n)$ *in* $\mathbb{V}_h\times\mathbb{H}_h$ *that satisfies the induction*

$$\begin{aligned} &\forall\psi_h\in\mathbb{H}_h, \qquad m_h\left(\psi_h,b_h^{n+1}\right)=\langle f^{n+1},\psi_h\rangle_{H^{-1},H_0^1}+\lambda\left(b_h^n,\psi_h\right),\\ &\forall\varphi_h\in\mathbb{V}_h, \qquad m_{*,h}(c_h^{n+1},\varphi_h)+a_{\rho,h}(b_h^{n+1},\varphi_h)=(g^{n+1},\varphi_h)+\lambda\left(c_h^n,\varphi_h\right), \end{aligned} \tag{4.3}$$

The parameter λ is the inverse of the time step, that is $\lambda=\tau^{-1}$. The resulting algebraic system has to be solved repeatedly and we choose to use a direct algorithm. Let us draw the attention here, that although the time-dependent problem (2.2) is ill-posed, it is but mildly ill-posed as illustrated in [4]. We refer to [23] for the definition of the ill-posedness degree. Hopefully, we shall be able to solve the discrete problem while avoiding the necessity of using any additional regularization other than the one require for the linear finite elements.

5 Numerical Examples

We describe two examples to assess the capability of the regularized mixed finite elements in simulating the solution of the steady system (2.1) where $\lambda = 0$. A particular care is paid to the convergence rates we observe for the finite elements. Computations are realized by means of the code `Freefem++` (see [14]), where a script is specifically dedicated to the pollution system. Then, we switch to the numerical checking of the unsteady problem (1.1)-(1.2).

5.1 The steady problem

The computational domain is here the square $(]-\frac{1}{2\pi}, 1-\frac{1}{2\pi}[)^2$. The dispersion parameter is permanently fixed to $d = 0.151$ while the reaction parameters $r(\cdot)$ and $r_*(\cdot)$ are piecewise constant. Each of them takes two possible values, 0.2 or 0.1 for $r(\cdot)$ and 0.4 or 0.2 for $r_*(\cdot)$. Both coefficients are depicted in Fig 5.1. Purple regions correspond to the greater values and the yellow strips are for the lower values. We are in the steady case, the one related to $\lambda = 0$.

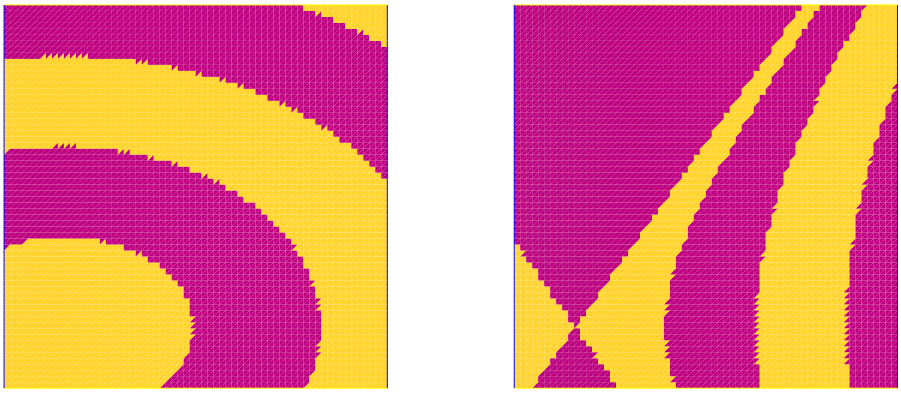

Figure 5.1: Reaction parameters $r(\cdot)$ and $r_*(\cdot)$.

We focus, in the first simulation, on the steady system where the exact solution (b, c) is supplied by

$$b(\boldsymbol{x}) = \cos(\frac{\pi}{2}x_1)\cos(\frac{\pi}{2}x_2), \qquad c(\boldsymbol{x}) = \sin(\frac{\pi}{2}x_1)\sin(\frac{\pi}{2}x_2).$$

The boundary of the domain is split into two portions. Along the horizontal edges, each the concentrations $b(\cdot)$ and $c(\cdot)$ is subjected to Neumann conditions while along the vertical walls Dirichlet and Neumann data are both enforced on $c(\cdot)$, $b(\cdot)$ being free from any boundary condition. Plots in Fig 5.2 are a super-imposition the isolines of the exact and the discrete solutions computed by the linear finite element method. They are obtained with a regularization parameter $\rho = 0.5$. They show the reliability of the regularizing tool to provide an approximation of $b(\cdot)$ with a good quality.

The variation of the *relative* errors $(b - b_h, c - c_h)$ versus the mesh-size h are depicted in the left panel Fig 5.3 for the suitably regularized solution ($\rho = 0.5$). The slopes of H^1-convergence curves for $b(\cdot)$ and $c(\cdot)$ are close to 0.91 and 1.03, respectively. Those related to the error in the L^2-norm are measured to $(1.41, 1.92)$. The convergence observed on $c(\cdot)$ is in agreement with the theory

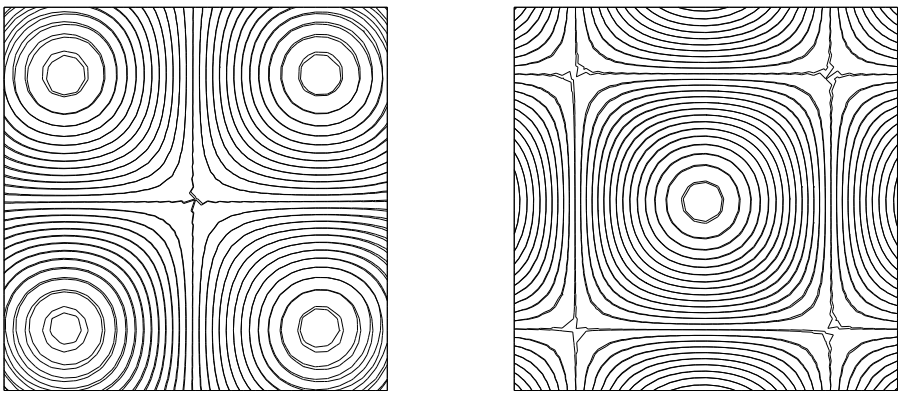

Figure 5.2: Isolines of the exact and the regularized computed solutions.

findings (see [5]). The variations of the error on $b(\cdot)$ are less coherent. In order to provide a complete insight on the quality of the approximation, we depict the variations of the same errors with respect to the L^∞-norm in the right plot of the same Fig 5.3. The convergence rate is evaluated to $(0.85, 1.96)$ for both tracers (b, c). Notice that so far there is no estimates proved on the maximum norm of the errors.

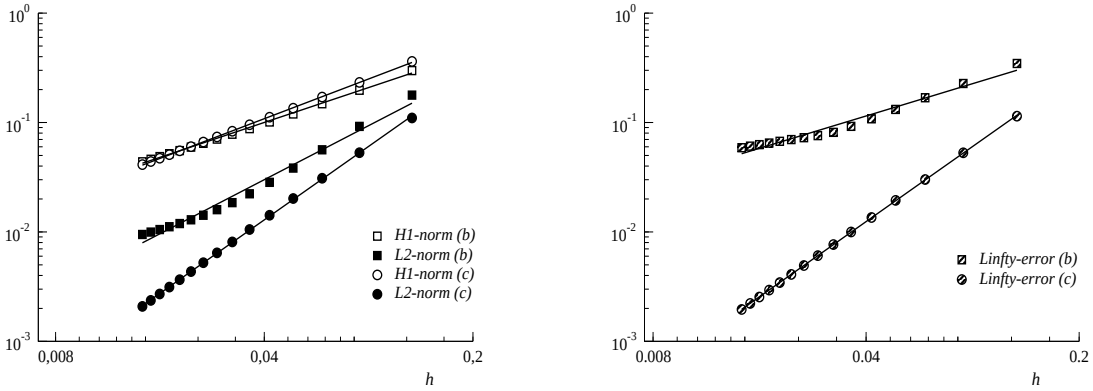

Figure 5.3: Convergence rates. The regularization parameter is fixed to $\rho = 0.5$

The issue of selecting the best possible regularization parameter is of course so important. Reader concerned with may find in the specialized literature many rules to achieve a judicious choice of this parameter. We refer for instance to [12, 13]. This is beyond the scope of the analysis we undertook here. Nevertheless, to figure out what happen for different values of that parameter we propose various plots in Fig. 5.4. In the two first rows the solution is under-regularized while in the last row it is over-regularized. What comes to sight is that the under-regularized density b_h starts to suffer from substantial inaccuracy at the border and in particular in the vicinity of the corners. The quality of c_h seems satisfactory. In the contrary, this BOD density c_h is clearly affected by over-regularization.

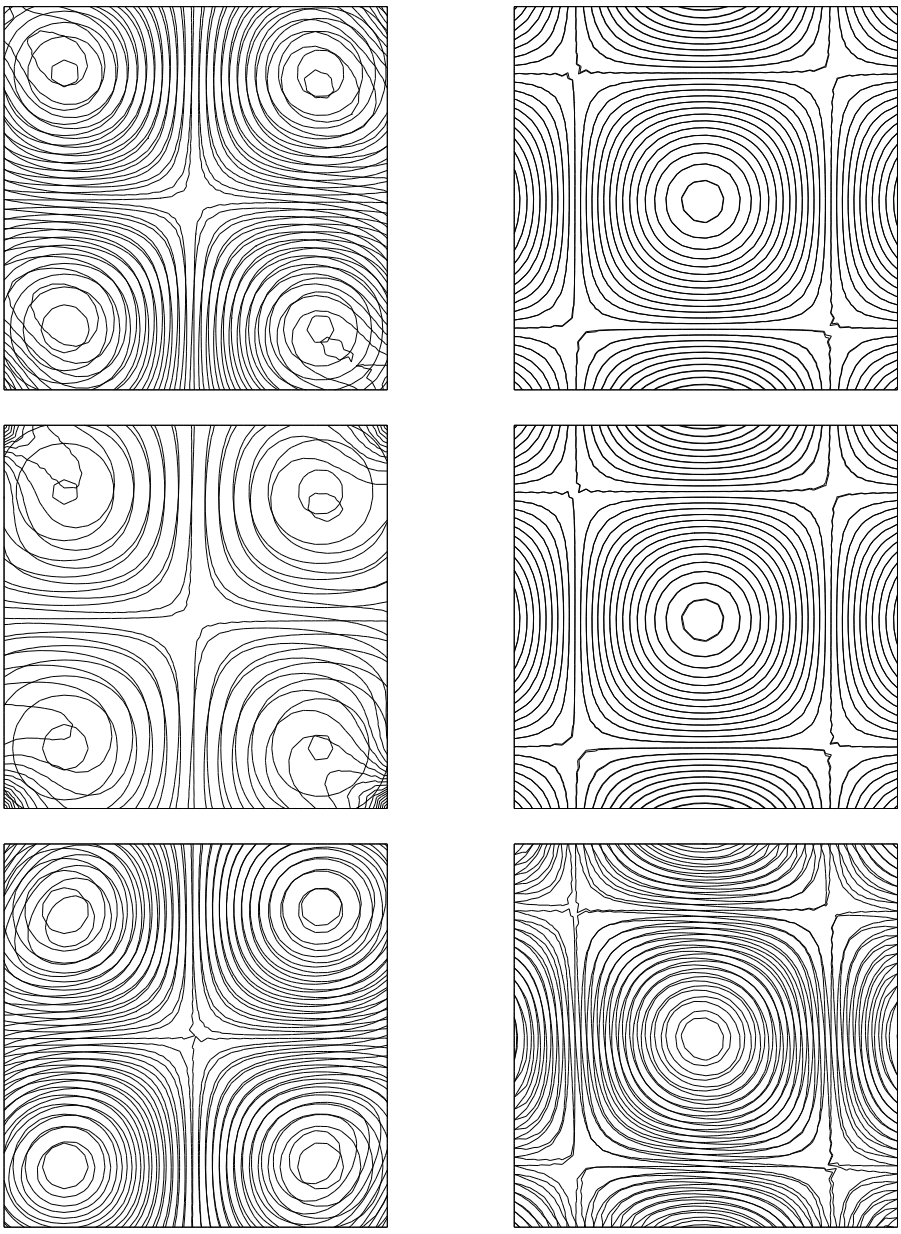

Figure 5.4: Under-regularized solutions with $\rho = 0.5$ (top) and $\rho = 0.05$ (middle). Over-regularized solution where $\rho = 5$ (bottom).

In the second steady test, we consider a more complex geometry. The computational domain looks like the Geneva lake (Leman lake) which is stretched in length along almost 60 (kms) and in large along 35 (kms). It is reconstructed from a Satellite picture of the lake (converted into portable gray-map format) shot at the border of France and Switzerland. The dispersion parameter is kept to $d = 0.151$ while the reaction parameters $r(\cdot)$ and $r_*(\cdot)$ are represented in the first row of Fig 5.5. The exact solution (b, c) is supplied by

$$b(\boldsymbol{x}) = -\ln\frac{r_1}{50} - \ln\frac{r_2}{50}, \qquad c(\boldsymbol{x}) = -r_1\ln\frac{r_1}{50} - r_2\ln\frac{r_2}{50}. \tag{5.1}$$

The functions $(r_i = r_i(\boldsymbol{x}))_{i=1,2}$ stand for the distance of the current point $\boldsymbol{x}$ to $(\boldsymbol{s}_i)_{i=1,2}$, two given fixed points. The functions (b, c) can be assimilated to the BOD and DO tracers due to a couple of polluting sources located at $(\boldsymbol{s}_i)_i$. We intend to reconstruct the densities $b(\cdot)$ and $c(\cdot)$ using finite element computations in the case of two sources located outside the domain and are however close to the boundary. The source $\boldsymbol{s}_1$ is situated up-north the lake while the second source $\boldsymbol{s}_2$ is placed down-south. The boundary part on which both Neumann and Dirichlet conditions are enforced on the DO density $c(\cdot)$ appears dark in first plots of Fig 5.5. Along the remaining (clear) portion, a Neumann type condition is fixed on both BOD and DO densities. Plots in the second row of Fig 5.5 depict the isolines of the computed solutions and may help the reader figure out where $\boldsymbol{s}_1$ and $\boldsymbol{s}_2$ are approximately positioned.
In this experience we run computations with an adaptation process of the mesh. We pursue the double advantages: calculate a better solution with a fixed number of vertices or degrees of freedom. An efficient mesh generation needs a metric. The construction of that metric uses the Hessian error indicator on the density b_h. We refer to [14] for a brief description of this error indicator and the way the adaptation procedure can be used within `Freefem`$_{++}$. The simulations are made when the parameter ρ equal 0.5. They start from a 'coarse' mesh with 170 triangles and 120 vertices and are stopped after ten refinements are realized. The 'refined' mesh has 5122 triangles and 2753 vertices. The meshes after five and ten refining are provided in the third row of Fig. 5.5. To have a better insight, the relative errors are recorded in Tab. 5.1 when evaluated in the energy, mass and maximum norms. They certify the reliability of the finite element method.

norm	H^1	L^2	L^∞
$(b - b_h)$	0.0825	0.0014	0.0130
$(c - c_h)$	0.0433	0.0001	0.0009

H^1	L^2	L^∞
0.0819	0.0014	0.0076
0.0425	0.0001	0.0007

Table 1: Finite element errors in the first (left) and the second (right) computations.

The symmetric test corresponds to a permutation of the boundary conditions. Neumann conditions are thus imposed on $b(\cdot)$ and $c(\cdot)$ along the dark portion of the boundary. Along the clear part we enforce Cauchy boundary conditions on $c(\cdot)$. Compared the previous test, the portion where Cauchy conditions are used on $c(\cdot)$ is substantially longer. Putting aside the singularities generated by the source term, specific instabilities may be born along the Cauchy boundary. This boundary is almost twice longer and we aim to achieve the same accuracy. After ten refining steps,

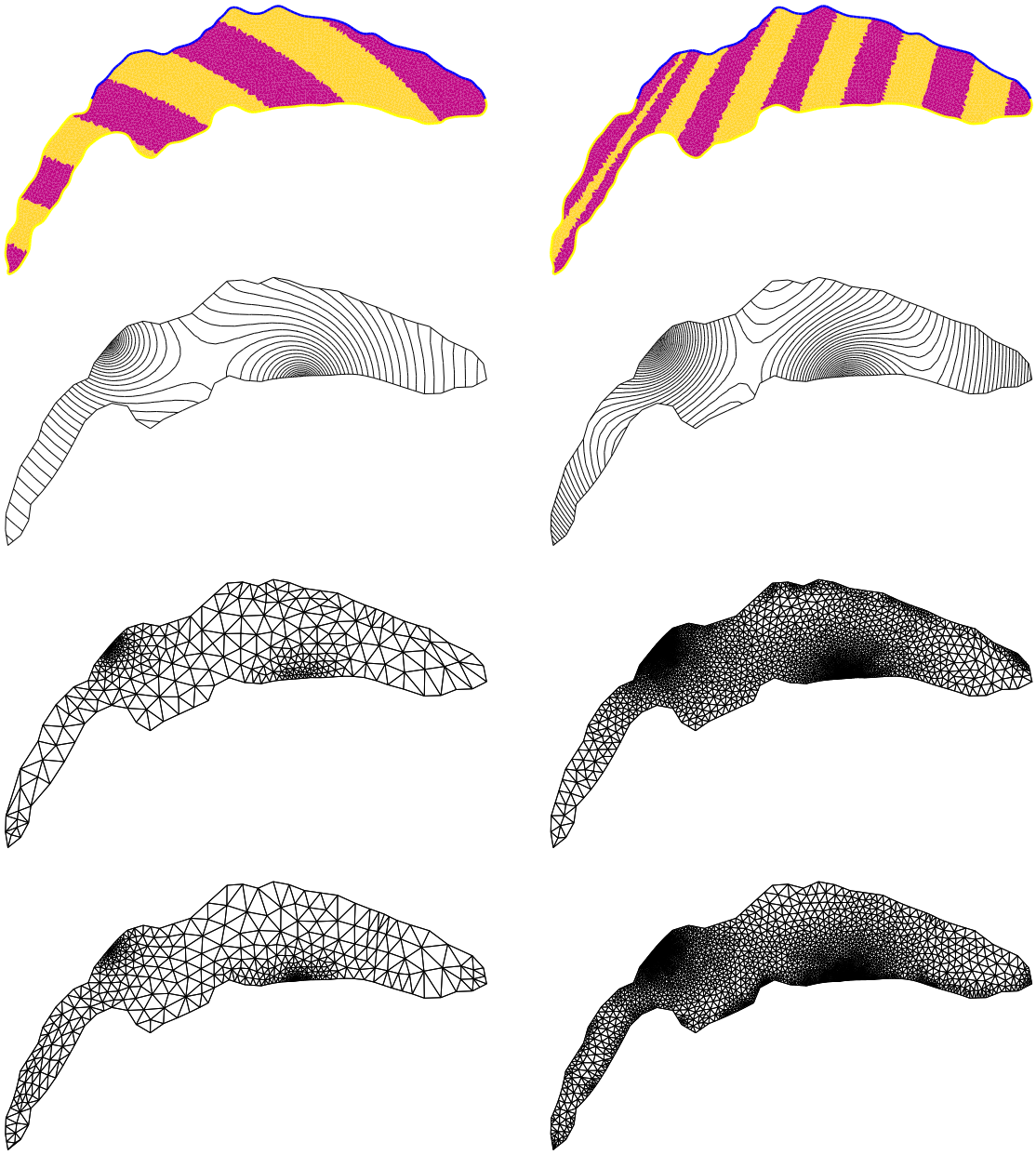

Figure 5.5: Reactions parameters. The steady computed concentrations. Adapted meshes after five and ten refinings (3rd and 4th rows).

the final mesh has 5371 triangles and 2910 vertices and the quality of the results we obtain is close to those obtained in the symmetric example. This is clearly displayed in Tab. 5.1. The only worthy observation to make after comparing different adapted meshes in the third and fourth row of Fig. 5.5 is that the refining seems sensitive to the boundary conditions. It is slightly moved toward the Cauchy part of the boundary. Look at the arm (left-bottom) of the lake to be convinced. It is more densely refined in the second computation where Cauchy condition is prescribed on the upper and lower boundaries (of that arm).

5.2 The unsteady problem

We begin by the illustration of the aptitude of the time scheme/finite element method to approximate a steady state. We therefore attempt to simulate the steady solution (5.1) of the last test in the the previous subsection, through the discretization of the time-dependent system (4.3). The geometry is the same Geneva lake. The boundary conditions are unchanged. Cauchy's conditions are imposed on $c(\cdot)$ on the whole lower part of the boundary and on the left portion of the upper part. The initial condition is put to zero. We use the adapted mesh, the one obtained at the end of the refining process in the steady calculations. It represented in the right panel of the fourth row in Fig. 5.5. It has thus 5371 triangles and 2910 vertices. We select the regularization parameter $\varrho = 0.5$ and the time step is fixed to $\tau = 0.5$. We hope to find out whether the ill-posedness has a negative effects on the final computations or not. Then, does the solution $(b(\cdot,t), c(\cdot,t))$ approximate the steady one when t grows high? The answer is affirmative. The computations are stopped after 100 time steps, when the final instant $t_F = 50$ is reached. Hence, we evaluate the gaps between the exact and the discrete solutions. They are recorded in Tab. 5.2. The results seems at least as satisfactory as those provided by a directly simulating the steady model. Comparing with the results displayed in the left table in Tab 5.1 demonstrates a better quality of the BOD density $b(\cdot)$ computed here. Intermediary dynamics, for both densities $b(\cdot,\cdot)$ and $c(\cdot,\cdot)$ are depicted in Fig. 5.6. They show the evolution for the computing to towards the steady state.

norm	H^1	L^2	L^∞
$(b - b_h)$	0.0394	0.0027	0.0041
$(c - c_h)$	0.0316	0.0002	0.0009

Table 2: Accuracy of the time scheme/regularized finite elements method.

In the second exmaple we deal with the real time-varying model. The exact solution (b, c) is thus time-dependent and is supplied by the expressions

$$b(t,\boldsymbol{x}) = \cos(\frac{\pi}{16}x_1 + 2\pi t)\cos(\frac{\pi}{16}x_2 + 2\pi t), \qquad c(t,\boldsymbol{x}) = \sin(\frac{\pi}{16}x_1 + 2\pi t)\sin(\frac{\pi}{16}x_2 + 2\pi t).$$

The time step is fixed to $\tau = 0.01$ and a quasi-uniform mesh is used with 5853 triangle and 3102 vertices. The first run is initiated with the regularization parameter put to $\rho = 0.5$. This value is the one that provided us with the more accurate numerical simulation in the steady case. The

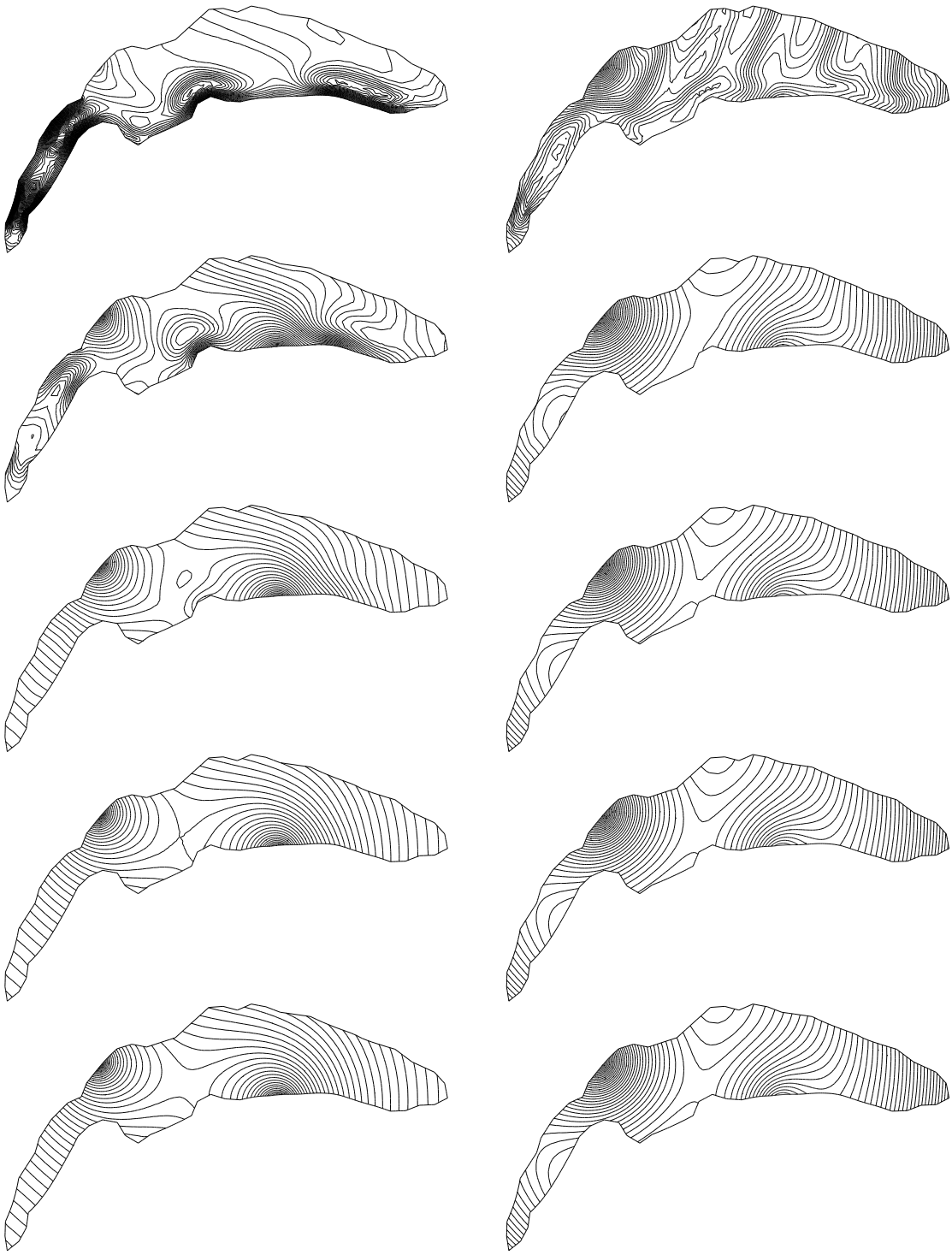

Figure 5.6: Convergence of the time-varying solution toward the steady state. Densities b_h and c_h at different times, $t = 10, 20, 30, 40$ and 50.

discrete tracers b_h^n and c_h^n obtained at the final instant $t_F = n\tau = 0.5$ ($n = 50$) are represented in the first plots of Fig. 5.7. The isolines of the density $c(\cdot,\cdot)$ seems to be nicely shaped. In the contrary those of $b(\cdot,\cdot)$ appear a little bit misshapen, the space between isolines is tight along the portion of the boundary where data are missing (on $b(\cdot,\cdot)$). The relative gap between $b(t_F,\cdot)$ and b_h^n is evaluated to 0.31 in the maximum norm while the one between $c(t_F,\cdot)$ and c_h^n is equal to 0.064. We then carried out a second experience with a higher regularization parameter that is $\rho = 20$. The isolines of b_h^n and c_h^n are represented in the second row of Fig. 5.7. The structure of the isolines of $b(\cdot,\cdot)$ are improved. Indeed, the maximum error on $b(t_F,\cdot)$ decreases to 0.015. In the other hand side, the isolines of $c(\cdot,\cdot)$ are apparently and slightly distorted, however without any substantial damage on the accuracy. Indeed, the gap between $c(t_F,\cdot)$ and c_h^n does not exceed 0.058 which is as a good result as the former one. To summarize We display in Tab. 5.2 the maximum norm of the errors at times $t_F = 0.5$ with the regularization parameters $\rho = 0.5$ and $\rho = 20$. Things happens as if there is a need of more regularization in the time dependent model than in the steady equation. This seems morally normal since adding the time derivative terms to the deoxygenation-reaeration system bring some more ill-posedness.

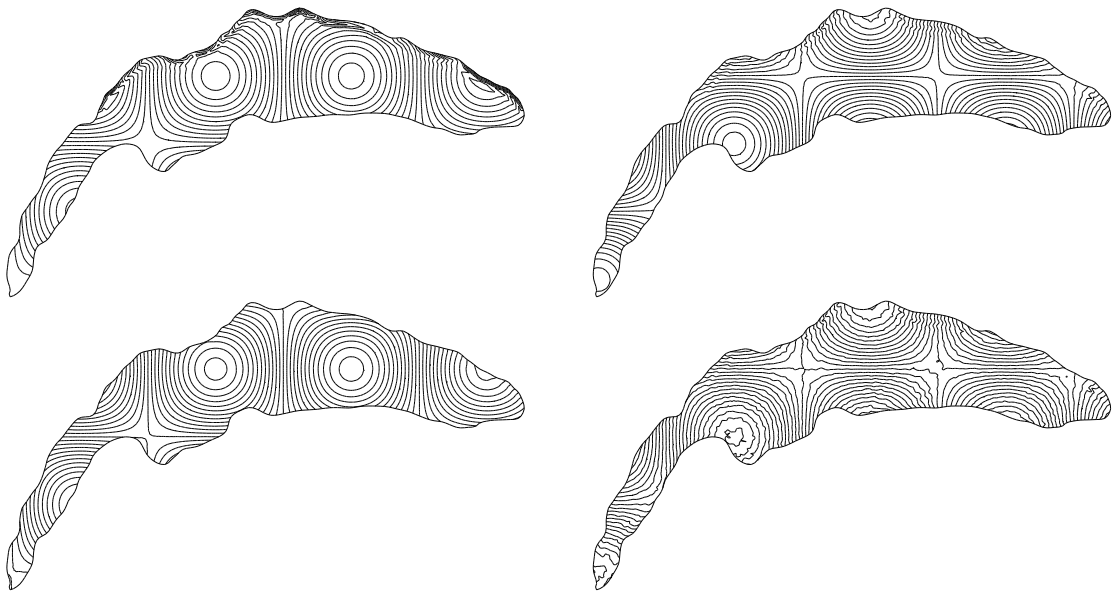

Figure 5.7: Time dependent solution. Under-regularized solution (top). Regularized solution (bottom).

$t(\varrho)$	0.5(0.5)	0.5(20)
$(b - b_h)$	0.309	0.015
$(c - c_h)$	0.064	0.058

Table 3: Gap between exact and discrete solutions.

6 Conclusion

The principle subject here is the analysis and the discretization of the inverse problem of data completion for the time-dependent dispersive deoxygenation-reaeration model. As illustrated earlier in [4], the most important feature of this problem is the ill-posedness which is intrinsically linked to the time dependency. As a consequence, uniqueness is the only result that hold true ; existence and stability both fail. Amazingly, the cause of the mathematical difficulties originates from the space-varying reaction parameters. This has been noticed in [5] for the steady counterpart of the problem. By the way, the well-posedness for that steady system established in that reference is in fact restricted to a particular class of the reaction coefficients. The main theoretical contribution of this work consists in showing that this limitation does not operate in the unsteady case and the identifiability we prove applies to arbitrary reactions.

In the numerical chapter, the examples we present for the data completion seem new. We do not know of any similar computational investigations. The model is approximated after putting together a mixed finite element method and an implicit Euler time-scheme. The ill-conditioning we are expected to inherit from the ill-posedness of the continuous problem is aggravated by the instability of the mixed finite element discretization. To remedy this specific weakness, we adopt the regularizing device recommended in [2]. This allows us to obtain some reliable results for the steady and unsteady versions of the deoxygenation-reaeration problem. Needless to say that the computational discussion led here is but a modest step in the numerical ground. We are called to sharpen our first observations and deepen the study of some important issues in particular with connection to the best regularizing strategy to apply. Is it necessary, for instance, to call for a second regularization method to cope with the ill-posedness specifically connected to the time derivatives of the BOD and DO densities? How the choice of the regularizing parameter(s) influences the solutions quality? How to automatically select the right parameter(s)? Many aspects remain therefore to be carefully investigated and more than one question are to be solved. The calculations achieved in [4] to check the ill-posedness shows that our problem can be related to the Volterra type equations. An exposition on the regularization artifices that fit in this class of problems can be found in [22, 15], for example. Before ending, we emphasize once again on the fact that, by the current study, we partially address a numerical subject that may be the milestone of number of challenges in environmental sciences and also of simply real-life problems. In summary, there remains a lot to be done, this is a substantial program which is actually under consideration.

References

[1] Adams, R. A., and Fournier, J. *Sobolev Spaces.* Academic Press, 2003.

[2] Amara, M., and Dabaghi, F. An optimal $\mathscr{C}^0$ finite element algoruthm for the 2D biharmonic problem: theoretical analysis and numerical results. *Numer. Math.*, 90 (2001), 19–46.

[3] Ben Belgacem, F. Uniqueness for an ill-posed reaction-dispersion model. application to organic pollution in stream-waters. *Inverse Problems and Imaging*, 6 (2012), 163 – 181.

[4] Ben Belgacem, F. Uniqueness in a cauchy problem for reaction-diffusion system and inverse source problems in water pollution. *M3AS 22* (2012), 1250029 (25 pages).

[5] Ben Belgacem, F., Bernardi, C., Hecht, F., and Salmon, S. Mixed finite element discretization of a model for organic pollution in waters. Part I. The problem and its discretization. *SIAM J. Numer. Anal.* (2013, submitted).

[6] Bernardi, C., Canuto, C., and Maday, Y. Generalized inf-sup condition for Chebyshev spectral approximation of the Stokes problem. *SIAM J. Numer. Anal. 25*, 6 (1988), 1237–1271.

[7] Bernardi, C., Girault, V., and Maday, Y. Mixed spectral element approximation of the Navier–Stokes equations in the stream-function and vorticity formulation. *IMA J. Numer. Anal. 12* (1992), 565–608.

[8] Brenner, S. C., and Scott, L. R. *Mathematical Theory of Finite Element Methods.* Springer, 2008, 12008.

[9] Brezzi, F., and Fortin, M. *Mixed and Hybrid Finite Element Methods.* Springer-Verlag, 1991.

[10] Brown, L. C., and Barnwell, T. O. *The Enhanced Stream Water Quality Models QUAL2E and QUAL2E-UNCAS: Documentation and User Manual.* Environmental Protection Agency, 1987.

[11] Ciarlet, P. *The Finite Element Method for Elliptic Problems.* North Holland, 1978.

[12] Engl, H. W., and Hanke, M.and Neubauer, A. *Regularization of inverse problems.* Mathematics and its Applications, 375. Kluwer Academic Publishers Group, Dordrecht, 1996.

[13] Hansen, P. C. *Rank-Deficient and Discrete Ill-Posed Problems: Numerical Aspects of Linear Inversion.* SIAM, 1987.

[14] Hecht, F. Freefem++, third edition, v 3.20. *Université Pierre et Marie Curie, Paris* (2011).

[15] Lamm, P. *A survey of regularization methods for first-kind Volterra equations.* In Surveys on Solution Methods for Inverse Problems, D. Colton, H. W. Engl, A. Louis, J. R. McLaughlin, W. Rundell, Editors Springer (Vienna, New York),, 2000.

[16] Nicolaides, R. Existence, uniqueness and approximation for generalized saddle point problems. *SIAM J. Numer. Anal.* (1982), 349–357.

[17] Okubo, A. *Diffusion and Ecological Problems: Mathematical Models.* Springer-Verlag, 1980.

[18] Pazy, A. *Semigroups of Linear Operators and Applications to Partial Differential Equations.* Springer-Verlag, 1983.

[19] Sawyer, C. N., McCarty, P. L., and Parkin, G. F. *Chemistry for Environmental Engineering and Science*. McGraw-Hill, 2003.

[20] Streeter, H., and Phelps, E. A study of the pollution and natural purification of the Ohio river. *US Public Health Bull. 146* (1925).

[21] Taylor, G. I. Dispersion of soluble matter in solvent flowing slowly through a tube. *Proc. Roy. Soc. A 219* (1953), 186–203.

[22] Tuan, V. K., and Gorenflo, R. Singular value decomposition of fractional integration operators in l^2-spaces with weights. *Journal of Inverse and III-posed Problems 3* (1993), 1–9.

[23] Wahba, G. *Ill posed problems: Numerical and statistical methods for mildly, moderately and severely ill posed problems with noisy data.* University of Wisconsin, Madison. Unpublished proceedings of the Delaware Conference on Ill Posed Inverse Problems, TR 595, 1980.

[24] Wang, S. T., McMillan, A. F., and Chen, B. An approximate solution to the advection-diffusion equation as applied to an estuary. *J. Hydrol. 48* (1980), 251–268.